Green Chemistry

Accepted Manuscript

ROYAL SOCIETY OF CHEMISTRY

www.rsc.org/greenchem

Ag–Fe_3O_4 Nanocomposites@Chitin Microspheres Constructed by in Situ One-pot Synthesis for Rapid Hydrogenation Catalysis

Bo Duan, Feng Liu, Meng He, Lina Zhang*

Department of Chemistry, Wuhan University, Wuhan 430072, China,

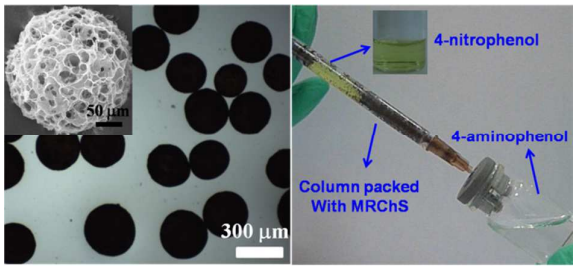

Ag-Fe_3O_4@chitin microspheres was developed as a retrievable catalysts and a potential chromatograpghy column packing materials for organic synthesis.

* To whom correspondence should be addressed. Phone: +86-27-87219274.

Fax: +86-27-68754067.E-mail: zhangln@whu.edu.cn, linazhangwhu@gmail.com

(L. Zhang).

$Ag–Fe_3O_4$ Nanocomposites@Chitin Microspheres Constructed by in Situ One-pot Synthesis for Rapid Hydrogenation Catalysis

Bo Duan, Feng Liu, Meng He, Lina Zhang*

Department of Chemistry, Wuhan University, Wuhan 430072, China

* To whom correspondence should be addressed. Phone: +86-27-87219274.

Fax: +86-27-68754067.E-mail: zhangln@whu.edu.cn, linazhangwhu@gmail.com

(L. Zhang).

Abstract

The fabrication of reusable and biodegradable materials from the renewable resources such as chitin is essential for a sustainable world. In the present work, chitin was dissolved in 11 wt% NaOH/4 wt% urea aqueous solution via freezing/thawing, and then chitin microspheres (RChS) were prepared by sol-gel transition method. Subsequently, novel magnetic Ag–Fe_3O_4@chitin microspheres (MRChS) were constructed successfully by in situ one-pot synthesis of Ag–Fe_3O_4 nanoparticles onto the RChS surface. The magnetic chitin microspheres displayed spherical shape with 3D-mesh structure, and had a narrow size distribution (150-400 μm). There were many micro- and nano-pores existed in MRChS, and the Ag-Fe_3O_4 nanoparticles were immobilized through anchoring with the acetyl amine groups of chitin in these pores. The MRChS microspheres were used as chromatography column packing material for "catalytic reaction column", and exhibited highly effective catalysis activity in the rapid transformation from 4-nitrophenol to 4-aminophenol. Moreover, the microspheres displayed a small hysteresis loop and low coercivity, as well as high turnover frequency (at least 10 times) without any loss of catalysis activity. Thus, MRChS could be fast removed out from the water under the magnetic field, leading to the easy recycle and reuse. Therefore, this is an environmentally friendly process, and would be highly beneficial to address the industrial requirements.

Keywords: silver nanoparticles, magnetic chitin microspheres, recycle catalysts, rapid catalytic reaction, environmentally friendly process

Introduction

Nowadays, the energy, resources and climate problems have drawn serious attention in view of the sustainability.[1, 2] Enhanced environmental consciousness has promoted the fusion of green chemistry with nanotechnology.[3-5] The purpose to improve the efficiency and lighten the environmental burden has made the nanoscience and nanotechnology one of the most burning issues. In the over-expanding field of nanomaterials research, noble metallic nanoparticles (Au, Ag, Pt, etc.) have garnered extensive attention due to their fascinating properties and applications in catalysis,[6, 7] sensors,[8, 9] imaging,[10, 11] photonics.[12, 13] Undoubtedly, catalysis is certainly among the most intensely studied problems.[14] Recently, the efficiency of the noble metallic catalysts in organic synthesis have been significantly improved by employing nano-sized catalysts due to their high ratio of surface area to volume, leading to the dramatic enhance in the contact between reactants and catalysts during the catalysis.[15, 16] However, the difficult recovery and reuse of the expensive nano-sized catalysts from the catalytic reaction systems by using traditional methods such as filtration and centrifugation results in the environmental and economic barriers.[17, 18] To overcome this issue, many efforts have been made to synthesize the magnetically retrievable nanocatalysts which possess high activity, selectivity, as well as meet the requirements of high accessibility with improved reusability.[19, 20] Unfortunately, they are very easy to aggregate to minimize their surface, leading to a remarkable reduction in their catalytic activities.[21, 22] To solve the problem of agglomeration, the immobilization of magnetic nanocatalysts on a solid

support has been regarded as one of the most efficient ways to overcome this drawback.[23, 24] Moreover, many solid supported catalysts have been successfully utilized for catalytic applications.[25] The materials with high surface area and good mechanical stability, such as carbon-based materials (carbon nanotubes,[26] graphene oxide,[27] and carbon-based nanofibers[28]), soluble and insoluble polymers,[29, 30] mesoporous silica,[31] metal oxide,[32] titania[33] etc, have been proved to be popular candidates for nanocatalysts supports. On the other hand, as far as concerned the call of the world for energy and sustainability, bio-inspired templating techniques using nature polymers (protein,[34] chitosan,[35] cellulose,[36, 37] etc) for catalysts supporters has become a valuable strategy.

It is worth noting that chitin is the second most abundant nature biopolymer after cellulose, existing mainly in the exoskeletons of crabs and shrimps.[38] Chitin has been reported to be a nature polysaccharide with significant biofunction.[39, 40] However, chitin remains perhaps the least exploited biomass source due to its intractable molecular structure which results in its recalcitrance to dissolution in most common solvent system.[41] To date, only a few solvents have been employed for chitin dissolution to prepare materials, including hexafluoroisoproanol (HFIP),[42] dimethylacetamide (DMAc)-LiCl mixture,[43] $CaCl_2$-MeOH[44] and ionic liquids.[45] In our laboratory, chitin was dissolved in an 11 wt% NaOH–4 wt% urea aqueous solution by using freezing (-30℃)/thawing cycles to prepare chitin hydrogels,[46] aerogels[47] and films.[48] However, the chitin microspheres fabricated directly from the chitin solution have been scarcely reported. Noticeably, chitin has been extensively

investigated as adsorbents for the metal extraction due to its large amount of acetyl amino groups, which serves as the chelation sites for metal ions.[49] Therefore, the chitin microspheres are a potential supporter for binding metal ions as well as for fabricating and stabilizing the metal nanocatalysts. Thus, we attempted to construct an easily retrievable chitin microsphere through a low-cost and energy-effective pathway by using the sol-gel transition (SGT) method. Subsequently, Ag-Fe_3O_4 nanocomposites were in situ one-pot synthesized onto the chitin microspheres to construct magnetic nanocatalysts. Furthermore, catalysis activity and retrievable properties of the nanocomposite microspheres were measured to evaluate their application in adsorption and catalyst fields. It is not hard to imagine that the regenerated chitin microspheres with external and internal surface area, porosity, hydrophilicity, and acetyl amino groups make it easy to fabricate and stabilize the functional nanoparicles for separation or catalysis thus showing potential applications in chromatographic separation and nanocatalysts fields. The utilizing of chitin from renewable resource to directly construct new microsphere via an environmentally friendly process would be meaningful on chemistry for a sustainable world.

Experimental Part

Materials

Chitin powder was purchased from Golden-Shell Biochemical Co. Ltd. (Zhejiang, China). The chitin powder was purified by a procedure described previously.[48] Firstly, 100 g chitin powder was treated with 400 g 5 wt% NaOH solution for 10 h under vigorous stirring. This suspension was then filtered and

125 washed with distilled water. Subsequently, the resulted chitin powder was treated with
126 400 g 7% (v/v) hydrochloric acid aqueous solution for 1 day to remove the residual
127 protein. After filtration and rinsing with distilled water, the treated sample was
128 dispersed in a 400 g 5 wt% NaOH solution for 1 day. The pigments were then
129 removed from the sample by using 1.7 wt % of sodium chlorite in 0.3 M sodium
130 acetate buffer (400 g) for 6 h at 80 °C, followed by washing with distilled water and
131 drying to obtain purified chitin powder. The degree of acetylation (DA) of the original
132 and purified chitin was calculated to be 90% and 94%, respectively, from the FT-IR
133 spectra according to

134 $$A_{1560}/A_{2875}=0.0125\times DA+0.2 \quad (1)$$

135 Where A_{1560}/A_{2875} is the ratio of the absorption bands at 1560 cm^{-1} and 2875 cm^{-1}.[50]
136 The weight-average molecular weight (M_w) was determined to be 53.4×10^5 in 5%
137 (w/v) LiCl/DMAc by dynamic light scattering (DLS, ALV/GGS-8F, ALV, Germany).
138 All of the chemical reagents were purchased from commercial sources in China, and
139 were of analytical-grade.

140 **Fabrication of regenerated chitin microspheres**

141 Sol-gel process means the transition of a system from a liquid (‘‘sol’’) into a
142 solid (‘‘gel’’) phase. In a colloidal suspension, the microspheres can aggregate into a
143 new phase to form the gel.[51, 52] In this work, the regenerated chitin microspheres were
144 fabricated by sol-gel transition method as follows. 7 g purified chitin powder was
145 dispersed into a 93 g mixture of NaOH, urea, and distilled water (11:4:85) by weight
146 with stirring to obtain a suspension. Subsequently, the suspension was frozen at -30

147 ^{o}C for 4 h, and then thawed at room temperature. The freezing/thawing cycle was
148 repeated twice to obtain a transparent chitin solution, with chitin concentration 7 wt%.
149 The chitin solution was degassed by centrifugation at 7200 rmp for 15 min at 0 ^{o}C. A
150 well-mixed suspension containing 100 mL of paraffin oils, 1.5 g of Tween 80 and 0.5g
151 of Span 80 were dispersed in a reactor. The resulting suspension was stirred at 500
152 rpm for 30 min, and then 20 mL of the chitin solution was dropped into the
153 suspension within 5 min. The suspension was kept stirring for 2h at the same stirring
154 speed at 0 ^{o}C, and then was heated to 25 ^{o}C with the same stirring speed for 0.5 h to
155 form regenerated chitin gels. Subsequently, 2 ml epichlorohydrin (ECH) was dropped
156 into the suspension within 10 min, and then was stirred at the same speed and
157 temperature for additional 1.5 h to completely crosslink the chitin gel. To the resultant
158 suspension, the dilute hydrochloric acid (10%) was added until pH = 7. After
159 removing the liquid paraffin, about 20 ml regenerated chitin microspheres in the
160 substratum were obtained, coded as RChS. The RChS microspheres were washed
161 with deionized water, and then ethanol successively for three times to remove the
162 residual paraffin oils, Tween 80 and Span 80. Finally, the microspheres were
163 freeze-dried or stored in 20% ethanol at 5 ^{o}C for characterizations.

164 **Fabrication of Ag-Fe_3O_4 / chitin nanocomposite microspheres**

165 Magnetic nanocomposite chitin microspheres were in situ one-pot synthesized by
166 redox reaction between Ag_2O and $Fe(OH)_2$ in the RChS microspheres as follows.
167 Desired amounts of $FeCl_2 \cdot 4H_2O$ were dissolved in 140 mL water, to which 15 mL
168 hydrated RChS (water content 80 wt%) was added, and then the suspension was

stirred for 1h with the protection of nitrogen at room temperature. Subsequently, the mixture was heated to 90 ℃ and a certain amount of 1M NaOH aqueous solution were mixed with the solution rapidly. The mixture was maintained at 90 ℃ in air with stirring after the addition of 10 mL aqueous solution containing desired amount of $AgNO_3$ for 2 min to obtain magnetic chitin microspheres, coded as MRChS. The MRChS microspheres were coded as M15, M30 and M45, according to the different concentrations of $FeCl_2$ at 15 mmol, 30 mmol, 45 mmol, corresponding to the amounts of 1 M NaOH/$AgNO_3$ to be 10 mL/0.212 g, 20 mL/0.424g and 30 ml /0.636 g, respectively. The MRChS microspheres were washed with deionized water until pH = 7. Finally, the MRChS microspheres were freeze-dried or stored in 20% ethanol at 5 ℃ for characterizations. The optical photomicrographs of the chitin microspheres were observed using a biological microscope (EX20, Sunny, China).

Characterization

Fourier-transform infrared (FT-IR) spectra of the microsphere samples were recorded on a Perkin-Elmer FT-IR spectrometer (model 1600, Perkin–Elmer Co. USA). The tested samples were prepared by the KBr-disk method. The wide-angle X-ray diffraction (XRD) was carried out on a XRD instrument (XRD-6000, Shimadzu, Japan) with Cu-Kα radiation (λ=0.154 nm). The XRD data were collected from 2θ = 10 to 90^o at a scanning rate of 2^o/min. X-ray photoelectron spectra (XPS) were recorded on a Kratos XSAM800 X-ray photoelectron spectrometer, using Mg Kα radiation as the excitation source. Thermo-gravimetric analysis (TGA) of the dry samples was carried out on a Pyris TGA linked to a Pyris diamond TA Lab System

(Perkin-Elmer Co., USA) at a heating rate of 10 K·min^{-1} from 30 to 700 ^{o}C under air atmospheres. Scanning electron microscopy (SEM) was performed on a FESEM (SEM, SIRION TMP, FEI) by using an accelerating voltage of 12 kV. The microspheres in the wet state were frozen in liquid nitrogen and freeze-dried under vacuum. The freeze-dried microspheres were sputtered with gold before observation. The high-resolution transmission electron microscopy (HRTEM) image was taken on a JEOL JEM 2010 FEF (UHR) microscope at 200 kV. The imbibed water of MRChS was exchanged to acetone, and then the microspheres were embedded with epoxy resin Epon812 (Shanghai Bioscience, Shanghai, China). After that, the embedded specimen was sectioned by a Leica Ultracut-E using a diamond knife to prepare approx.80 nm-thick sections. These samples were sputtered with carbon before HRTEM test. The definite size distribution of RChS and MRChS was determined with a Mastersizer 2000 laser particle size analyzer (Malvern, UK).

Nitrogen physisorption measurements at 77 K were performed by a Micromeritics AsAp2020 (USA), and Brunauer-Emmett-Teller (BET) and Barrett-Joyner-Halendar (BJH) analyses were done by software. The microspheres were degassed at 105 ^{o}C in vacuum to remove all the adsorbed species. BET analysis was performed for relative vapor pressures of 0.05-0.3. The BJH analysis was performed from the desorption branch of the isotherms.

The magnetic properties of the composite microspheres were measured with a vibrating sample magnetometer (VSM, Lake Shore, 7304, USA) at 25 ^{o}C, and the hysteresis loop was obtained in a magnetic field that varied from -0.6 to +0.6 T.

Catalytic Activity Assays

The microspheres used for catalytic reduction were obtained via exchanging the water in hydrated microspheres to acetone and then drying under vacuum at ambient temperature for 24 h. The catalytic activity of Ag-Fe_3O_4/chitin microspheres was evaluated by using the reduction of 4-nitrophenol (4-NP) to 4-aminophenol (4-AP) in a quartz cell at 25 °C, monitored using UV–visible spectroscopy (UV-6, Shanghai Meipuda instrument Co., LTD., Shanghai, China). More specifically, 0.75 mL of fresh $NaBH_4$ aqueous solution (0.4 M) was mixed with 1.5 mL aqueous dispersion of MRChS (Ag-Fe_3O_4@chitin) microspheres at 50 mg/L. Subsequently, 0.75 mL of 4-NP aqueous solution (4×10^{-4} M) was added. As a result, the concentration of 4-NP and $NaBH_4$ in the reaction solution was 1×10^{-4} and 0.1 M, respectively. The catalytic reaction was monitored at decided time intervals. The control experiment was carried out under identical condition except that the Ag-Fe_3O_4@chitin microspheres aqueous dispersion was replaced with 50 mg/L chitin microspheres. At the end of the reaction, the catalyst was separated from the reaction system using an external magnet, washed three times with ethanol and dried at room temperature for the next cycle. Additionally, the RChMS microspheres suspended in distilled water were packed in an injector (1 ml) which acted as a reaction column to form a 1.5cm long gel bed. The column was equipped with a glass collector, and a piece of cotton wool was placed at the bottom of the injector to prevent the outflow of the MRChS. The mixture solution of $NaBH_4$ (0.1 M) and 4-NP (1×10^{-4} M) was added in the injector from the top and squirted through the MRChS packing. The product was gathered in the glass collector.

Results and Disscusion

Green process of the preparation for the magnetic chitin microspheres

The process for the preparation of the chitin microspheres (RChS) was described in Scheme S1. Firstly, the chitin solution was prepared by using the aqueous NaOH/urea via freezing/thawing method, which is an environmental friendly solvent. Moreover, it was very easy to give a sol-gel transition for chitin solution directly through heating up to 20 ℃.[47] Secondly, the chitin droplets were heated to 25 ℃ to proceed the "sol -gel" transition. Unfortunately, the chitin microspheres regenerated directly with heating displayed a non-homogeneous distribution and nonspherical shape (See Fig S1a). It might result from its poor mechanical properties. To construct the chitin microspheres with a stronger network structure, a further crosslink was performed. As expected, the chitin microspheres crosslinked with ECH (see Scheme. S2) displayed a perfectly well-defined spherical shape with porous structure (see Fig. S1b and S2).The preparation of RChS was a green process, which included the direct utilization of the renewable resource, the dissolution in the environmental friendly NaOH-urea aqueous solvent, no evaporation of any chemical agents, as well as low cost and clean emulsification pathway. It was noted that the dissolution and regeneration of the chitin was a physical process through non-covalence, and the DA value hardly changed.[48]

The FTIR spectra of the regenerated chitin microspheres (see Fig. S3) showed there were large amounts of acetyl amino groups (DA=91%, calculated with eqn 1), which could serve as anchoring sites for the metal ions.[49] Thus, the Fe^{2+} can be easily

absorbed and stabilized onto the chitin microspheres through the strong interaction with these acetyl amino groups of chitin. Moreover, by adding alkaline and $AgNO_3$, the $Fe(OH)_2$ reacted with Ag_2O to give magnetic Ag-Fe_3O_4 nanocomposites in the chitin microspheres, leading to the formation of the magnetic MRChS microspheres. Herein, the entire preparation of the MRChS composite in aqueous solution was finished under clean and moderate condition, which was also an environmentally friendly method. Moreover, the original feature (such as metal ions absorbent) of chitin was maintained in the magnetic microspheres, leading to the excellent candidate for the nanoparticle supporters.

Structure and morphology of the magnetic chitin microspheres

The optical photomicrographs and size distribution observed with the laser particle size analyzer for the RChS and MRChS microspheres are shown in Fig. 1. RChS and MRChS (M30) at the swollen state had average diameters about 251 μm and 253 μm, respectively, and displayed the narrow size distribution which fitted the Gaussian distribution on the whole (Fig. 1b, d). It was noted that both RChS and MRChS exhibited the same spherical shape and size distribution. This could be explained that the synthesis reaction of Ag-Fe_3O_4 occurred in the pores of the chitin microspheres, so the morphology of the composite microspheres changed hardly, compared to the original one. From the analysis of the XRD patterns (See Fig. S4), the Ag-Fe_3O_4@chitin composite microspheres displayed a typical α-chitin structure.[48] Distinct peaks of MRChS at 2θ of 38.1, 44.3, 64.4, 77.5 and 81.6° were assigned to the (111), (200), (220), (311) and (222) planes of Ag, whereas the 2θ = 30.2, 35.6,

57.2, and 62.6° to (220), (311), (511) and (440) were ascribed to planes of Fe_3O_4, respectively. The diffraction peaks of Ag appeared to be much stronger than those of Fe_3O_4, suggesting that the crystallization of Fe_3O_4 nanoparticles was not so perfect as that of Ag.[17] In view of the results in Fig.1 and S4, the MRChS were consisted of chitin, Ag and Fe_3O_4.

To clarify the morphology of the chitin microspheres and the distribution of Ag-Fe_3O_4 nanoparticles on their surfaces, the microspheres were observed by SEM. The SEM images of the surfaces of RChS and MRChS are shown in Fig. 2, S2 and S5. The morphology of RChS and MRChS displayed the spherical shape (Fig. 2) and 3D network structure with interconnecting pores (see Fig. S2 and S5). Obviously, there was no essential change for the MRChS morphology during the growth of Ag-Fe_3O_4 nanoparticles compared with RChS. The surface of RChS exhibited microporous structure with an apparent mean diameter of 3-20 μm for the micropores (measured from the Fig. 2). The pore formation was a result of the phase separation induced by the occupying H_2O during sol-gel process, where the solvent-rich regions contributed to the pore formation.[53] However, as shown in Fig. 2b, c and d, the MRChS composite microspheres (M15, M30 and M45) exhibited relatively denser surfaces than that of RChS. It was further confirmed that Ag-Fe_3O_4 nanoparticles could be readily impregnated into the pores and/or channels of the chitin matrix through bounding to the chitin macromolecules as a result of the chelation of acetyl amino groups. The Ag-Fe_3O_4 nanoparticles were extensively and homogeneously dispersed on the surface of the chitin microspheres (See Fig. S5b, c and d). This suggested that the unique 3D-

porous structure and abundant acetyl amino groups of RChS provided a good platform for the immobilization of Ag-Fe_3O_4 nanoparticles, which were deposited and anchored in the chitin matrix during the redox reaction process between $Fe(OH)_2$ and Ag_2O through being immersed in salt and alkaline aqueous solution .

The SEM could only be used to confirm the micro-sized porous structure appeared on the surface of the chitin microspheres. Thus, the surface area and corresponding nano-sized porous structure of the Ag-Fe_3O_4 nanocomposites@chitin microspheres were determined by using N_2 adsorption-desorption method. Fig. 3 shows nitrogen adsorption and desorption isotherms and Barrett-Joyner-Halendar (BJH) pore size distribution of RChS, M15, M30, and M45. Both RChS and MRChS exhibited a type I H3 hysteresis loop according to the IUPAC and BDDT classification, as the adsorption branch is parallel to the P/P^0 over a large extent .[54] The BET surfaces area, pore volume and pore size of RChS and MRChS were calculated, and the data are summarized in Table 1. The result revealed that inner of the microspheres exhibited the nano-sized pores, and the most probable values of pore size ranged from 10 to 50 nm (Fig. 3b), indicating that MRChS maintained its initial nanoporous structure after the immobilization of Ag-Fe_3O_4 nanoparticles. The decrease in surface area and pore volume of MRChS compared with RChS indicated that the Ag-Fe_3O_4 nanoparticles occupied in the pores of the chitin microspheres.

TEM and high resolution TEM (HRTEM) were used to study the microstructure of the magnetic chitin microspheres in more detail. Fig. 4 shows TEM and HRTEM images of the magnetic microspheres of M10 (a), M20 (b) and M30 (c). The

Ag-Fe_3O_4 nanocomposites with spherical shape and mean diameter of 10-40 nm were dispersed uniformly in the chitin matrix. The size of the Ag-Fe_3O_4 nanoparticles in these microspheres changed slightly with an increase of the Ag-Fe_3O_4 content (see Fig 4a, b, c, and Fig. S6). This could be explained that the acetyl amino groups on the RChS surface captured a certain amount of the Fe^{2+}, which could terminate the reduction action between $Fe(OH)_2$ and Ag_2O, and the micro- and nano-sized pores of the chitin martrix acted as micro-chambers to limit the growth of the Ag-Fe_3O_4 nanoparticles. In our findings, the preparative chitin microspheres could be used as an excellent metallic nanoparticle supporter. From the HRTEM image and the corresponding energy-dispersive spectrum (EDS) in Fig. 4d, e, the clear crystalline lattices were attributed to (111) (d=0.235 nm), (200) (d=0.203 nm) phases of Ag, and (311) (d= 0.251 nm), (511) (d=0.162 nm) phases of Fe_3O_4. The results confirmed the successful synthesis of Ag-Fe_3O_4 nanoparticles in this manner. Interestingly, there were some rod-like crystals of Fe_3O_4 around the spherical Ag-Fe_3O_4 nanoparticles. This could be explained that from the EDS curve for the rod-like crystal (see Fig. S7b), there were only C (sputtered carbon), O and Fe elements in this crystal, so these nanocrystals were made of Fe_3O_4, which should result from the oxidation of $Fe(OH)_2$.[55]

More detailed information regarding the chemical and bonding environment of the chitin microspheres and Ag-Fe_3O_4 nanoparticles were ascertained using X-ray photoelectron spectroscopy (XPS). Fig. 5a shows the fully scanned spectra in the range of 0-800 eV. These results from overview spectra demonstrated that C, O, N ,

Ag and Fe existed in the magnetic microsphere of M30, while only C, O and N appeared in RChS. Fig. 5b shows the XPS spectrum in Ag 3d region of M30. Two peaks at 373.8 eV and 367.8 eV were well corresponded with $Ag3d_{5/2}$ and $Ag3d_{3/2}$ binding energies, respectively, in good consistent with the reported data of Ag^0.[7] On the other hand, the binding energies at 724.6 and 711.1 eV in Fig. 5c were attributed to $2p_{1/2}$ and $2p_{3/2}$ of Fe, which was a typical core level spectrum of Fe_3O_4 with broad peaks, confirming the formation of Fe_3O_4.[56, 57] Interestingly, all peaks of Ag and Fe were shifted to lower binding energies compared with the reported characteristic metallic Ag^0 peaks at 374.1 and 368.1 eV and Fe_3O_4 peaks at 725.0 and 711.5 eV.[55, 58] However, the peak of N in M30 was shifted obviously to the higher binding energy (398.8 eV) compared with RChS (398.3 eV) (Fig. 5d). These results indicated that the N in acetyl amino groups acted as the anchorage and stabilization for Ag-Fe_3O_4 nanoparticles, leading to their immobilization on MReChS. This might be explained that the transformation of the coordination electronic from N to Ag-Fe_3O_4 nanoparticles resulted in a decrease of the binding energy for Fe and Ag, but an increase for N. The high resolution XPS spectra for the C1s region around 285 eV is shown in Fig. 5e.The three types of peak at 286.8 eV, 285.4 eV, and 283.7 eV were assigned to the each carbon atoms of the C=O group, the C-O or C-N group and C-C or C-H in chitin, respectively.[59] The similar three peaks of the C1s for RChS and M30 suggested that the Ag-Fe_3O_4 nanoparticles did not attach the C atoms of chitin. Fig. 5f shows the spectra of O1s for the bare RChS and the Ag-Fe_3O_4/chitin composite microspheres (M30). The shape of a wide and asymmetric peak of O1s spectrum for

368 both RChS and M30 indicated that there was more than one chemical state according
369 to the binding energy. Three peaks of RChS O1s spectrum were identified: at 532.2 eV,
370 assigned to O-C-O; at 531.3 eV, assigned to C–O-H and C-O-C; 530.2 eV assigned to
371 N-C=O, respectively.[60] For the M30, the O1s peak can be generally regarded as a joint
372 contribution of the RChS and Ag-Fe_3O_4 nanocomposites, indicating a clear difference
373 with that of RChS in its lower tails. The peak at 530.4 eV was ascribed to the anionic
374 oxygen in Fe_3O_4 (Fe-O or Fe=O).[61] Interestingly, the N-C=O peak at 529.4 eV of M30
375 obviously shifted to lower binding energy compared with that of RChS (530.2 eV),
376 suggesting that the O atom of N-C=O group served as anchoring sites together with N
377 atom for Ag-Fe_3O_4 nanoparticles. Namely, the acetyl amino groups were the
378 anchoring sites for the Ag-Fe_3O_4 nanoparticles.

379 **Formation mechanism of Ag-Fe_3O_4@chitin microspheres**

380 On the basis of the above experimental results and theory analysis, a possible
381 mechanism for the construction of Ag-Fe_3O_4@chitin microspheres is proposed in
382 Scheme 1. There were many micro- and nano-pores in the chitin microspheres, as
383 shown in Fig 2 and 3. The large amounts of acetyl amino groups existed in the pores
384 of chitin microspheres (Scheme 1a), supported by the results in Fig. 5 and S3. Thus,
385 Fe^{2+} was absorbed and stabilized quickly into the pores through binding with acetyl
386 amino groups. Subsequently, the $Fe(OH)_2$ particles were generated with the addition
387 of alkalinity (Scheme 1b). When $AgNO_3$ was added into the alkaline suspension, the
388 redox reaction between Ag_2O and $Fe(OH)_2$ took place rapidly, leading to the in situ
389 one-pot synthesis of the Ag-Fe_3O_4 nanoparticles in the micro- and nano-sized pores

(Scheme 1c), supported by the results in Fig. 3, 4, 5 and S4.

The Ag-Fe_3O_4@chitin nanocomposites was fabricated through the redox reaction between $Fe(OH)_2$ and Ag_2O as follows. [55]

$$Fe^{2+} + 2OH^- \rightarrow Fe(OH)_2 \quad (2)$$

$$2Ag^+ + 2OH^- \rightarrow Ag_2O + H_2O \quad (3)$$

$$2Ag_2O + 6Fe(OH)_2 \rightarrow 2Fe_3O_4 + 4Ag + 6H_2O \quad (4)$$

In our findings, the pores in the chitin microspheres served as microreacters for the synthesis and growth of Ag-Fe_3O_4, leading to the formation of the Ag-Fe_3O_4 nanoparticles with narrow size distribution. The acetyl amino groups as an anchoring sites captured the Ag-Fe_3O_4 nanoparticles (Scheme 1c), supported by the results in Fig. 5. All of these results gave the insight that (1) the heterostructures were composed of Ag-Fe_3O_4 nanocomposites and chitin; (2) the acetyl amino groups on chitin microspheres acted as the anchoring sites for the Ag-Fe_3O_4 nanoparticles; (3) the porous microspheres were used as micro-reactors to supply not only cavities for the constructiob of the nanoparticles, but also a shell to protect the nano-structure and catalysis activity.

Magnetic properties

The magnetic properties of these materials are critical to ensure their applications. Fig. 6a shows the magnetization of M15, M30 and M45 as a function of the magnetic field at 298 K. The magnetization of these MRChS microspheres increased considerably with an increase of the Ag-Fe_3O_4 nanocomposites. Though, the magnetization of the composite microspheres in each sample was weak and showed a

lack of saturation, they exhibited a small hysteresis loop and low coercivity, suggesting a superparamagnetic behavior. The saturation magnetization of M15, M30, M45 obtained from the hysteresis loop was 2.41, 2.81 and 3.42 emu/g, respectively, depending on the effective mass of the Fe_3O_4 nanoparticles. To further investigate the magnetic response of the MRChS, the magnet was used to attract the microspheres in water. Fig. 6b, c and d show photographs of the MRChS dispersion in water and the attraction behaviors induced by the magnet. As shown in Fig. 6b, the MRChS were drawn rapidly to attach on the surface of the magnet within 5 sec, and were completely attracted to collect from the water in the jar within 13 sec (Fig. 6c and Video 1). Obviously, the magnet can be employed efficiently to recycle the MRChS. Moreover, the magnetism of the MRChS was not only strong enough to separate themselves out from the action system with the help of an external magnetic field, but also beneficial for the easy redispersion for reuse (see Video 1). Therefore, MRChS could be fast removed out from the water under the magnetic field, leading to the easy recycling and reuse. The convenient recycle of the magnetic microspheres conformed to the call of the green chemistry.

Catalytic activity

It is well-known that metallic silver nanostructures are excellent catalysts with high activity and selectivity. Thus, the silver immobilized on a porous microspheres support could serve as a practical recyclable catalyst and chromatograph packing materials towards many reactions. In our findings, the reduction of 4-nitrophenolate (4-NP) to 4-aminophenolate (4-AP) in the presence of $NaBH_4$ was chosen as model

reactions to evaluate the catalytic activity of the as-prepared Ag-Fe_3O_4@chitin catalyst. Usually, the 4-NP aqueous solution has a maximum absorption at 317 nm in the UV-vis spectrum which is remarkably red-shifted to 400 nm when it has been treated with an aqueous solution of $NaBH_4$, corresponding to a color change from light yellow to bright yellow.[62] The absorption at 400 nm reflects the formation of 4-nitrophenolate ions, owing to an increase in solution alkalinity, caused by the addition of $NaBH_4$.[63] The reaction conversion can be calculated from C/C_0, which is measured from the relative intensity of UV-vis absorbance (A/A_0) at 400 nm.[28] Herein, C is the concentration of the 4-NP at the reactant and C_0 is the initial concentration. Fig. 7a shows the catalytic efficiency of the reduction reaction of MRChS on 4-NP as a function of time. After the addition of Ag-Fe_3O_4@chitin into the system, the absorption intensity of 4-NP at 400 nm decreased rapidly with time, and a new peak at 295 nm appeared, indicating the formation of 4-AP,[64] which was accompanied with its perceptible color change. For comparison, the control experiment was conducted with a mixture of 4-NP, $NaBH_4$ reducing agent and chitin microspheres without Ag-Fe_3O_4@chitin (Fig. 7b). The solution remained bright yellow with a constant absorption peak at 400 nm for the control experiment, indicating that the catalytic reduction of 4-NP did not occur. However, when the Ag-Fe_3O_4@chitin microspheres were added into the reaction mixture such as M15, M30 and M45, the C/C_0 values or the peak intensity at 400 nm of 4-NP rapidly decreased with an increase of the reaction time. In this experiment, the $NaBH_4$ was used in large excess to 4-NP, and can be considered as constant during the reaction

period. So the pseudo-first-order kinetics can be applied to evaluate the reaction rate constants. The reaction kinetics can be described as[34]

$$\ln(C/C_0) = -kt, \quad (5)$$

Where k is the apparent first-order rate constant (min^{-1}), t is reaction time. Fig. 7c shows a linear relationship for $\ln(C/C_0)$ against t in the reduction catalyzed by the heterostructures following the pseudo-first-order kinetics. The reaction rate constants were calculated to be k~0.3139 min^{-1} for M45, k~0.2621 min^{-1} for M30 and k~0.2236 min^{-1} for M15. This indicated that the catalytic efficiency was enhanced with the increasing content of silver nanoparticles in the Ag-Fe_3O_4@chitin microspheres (see Fig. S9).

Stability and recyclability of catalysts are of great importance for the practical applications. Fig. 7d shows the catalytic activity of M30 (50 mg/L) for the reduction of 4-NP with 10 successive times of cycling uses. The results for the different times of cycling uses were very similar and the catalytic activity changed hardly, indicating MRChS possessed high turnover frequency (at least 10 times) without any loss of catalysis activity. The recyclability of the catalyst may result from the highly efficient stabilization of the Ag-Fe_3O_4 nanoparticles immobilized in the chitin microsphere. Interestingly, considering the high recycled frequency, favorable size (150-400 μm) and porous structure of the magnetic microspheres, it would greatly promote the application of the MRChS in the catalysis field.

The photograph for the MRChS acting as chromatographic packing materials in injector for rapid catalysis is shown in Fig. 8. When the yellow solution (4-NP and

$NaBH_4$) was syringed through the MRChS packing, the Ag immobilized on the MRChS efficiently catalyzed the reduction of 4-NP to 4-AP, and immediately, the colorless product of 4-AP appeared in the collector (also seen in Video 2). The highly efficient catalytic activity and the facile application of the MRChS are important in the catalysis field. Moreover, all samples had adequate thermal stability because the decomposition did not occur below 200 ℃ (see Fig. S9). This is important for the huge potential application of the nanocomposite catalysts because thermal stability of catalysts is necessary for many catalytic reactions. Therefore, this work would supply a broad pathway to immobilize the noble metallic nanocatalysts for the further industrial application. It was worth noting that chitin could be biodegraded in the soil, and could serve as plant growth regulator to promote the plant growth even after they had been discarded.[65]

Conclusion

Chitin microspheres having acetyl amino groups were prepared successfully in an aqueous system by sol-gel transition method via a green pathway. The Ag-Fe_3O_4 nanoparticles with mean size 10-40 nm were in situ one-pot synthesized in the micro- and nano-pores of the microspheres through strong interaction between Ag-Fe_3O_4 and chitin. The porous microspheres were used as micro-reactors to supply not only cavities for the formation of the nanoparticles, but also a shell to protect the nano-structure and catalysis activity. Moreover, the acetyl amino groups of chitin served as anchoring and stabilizing agent to trap the Ag-Fe_3O_4 nanoparticles to immobilize in the chitin microspheres. The magnetic composite chitin microspheres

were proved to be not only highly efficient for the catalytic reaction from 4-NP to 4-AP, but also an easily recyclable and reusable catalyst. The chitin microspheres containing Ag-Fe_3O_4 nanoparticles would have great potential in industry as a broad platform for metallic nanoparticle immobilization and for rapid catalysis. Both the fabrication and use of the magnetic composite microspheres were very simple and convenient. Therefore, this is an environmental friendly material and process, which is accorded to the sustainability.

ACKNOWLEDGMENTS. This work was supported by National Basic Research Program of China (973 Program, 2010CB732203), the Major Program of National Natural Science Foundation of China (21334005) and the National Natural Science Foundation of China (20874079).

References

1. D. S. Su, S. Perathoner and G. Centi, *Chem. Rev.*, 2013, **113**, 5782-5816.
2. S. Chaemchuen, N. A. Kabir, K. Zhou and F. Verpoort, *Chem. Soc. Rev.*, 2013, **42**, 9304-9332.
3. S. Shylesh, V. Schünemann and W. R. Thiel, *Angew. Chem., Int. Ed.*, 2010, **49**, 3428-3459.
4. V. Polshettiwar and R. S. Varma, *Green Chem*, 2010, **12**, 743-754.
5. V. Polshettiwar, R. Luque, A. Fihri, H. Zhu, M. Bouhrara and J.-M. Basset, *Chem. Rev.*, 2011, **111**, 3036-3075.
6. A. Mohanty, N. Garg and R. Jin, *Angewandte Chemie International Edition*,

2010, **49**, 4962-4966.

7. T. Wu, L. Zhang, J. Gao, Y. Liu, C. Gao and J. Yan, *J. Mater. Chem. A*, 2013, **1**, 7384-7390.

8. L. Wang, H. Dou, Z. Lou and T. Zhang, *Nanoscale*, 2013, **5**, 2686-2691.

9. T. Gao, Y. Wang, K. Wang, X. Zhang, J. Dui, G. Li, S. Lou and S. Zhou, *ACS Appl. Mater. Interfaces*, 2013, **5**, 7308-7314.

10. R. Gavara, J. Llorca, J. C. Lima and L. Rodriguez, *Chem. Commun.*, 2013, **49**, 72-74.

11. C.L. Liu, T.M. Liu, T. Y. Hsieh, H. W. Liu, Y.S. Chen, C. K. Tsai, H. C. Chen, J. W. Lin, R. B. Hsu, T. D. Wang, C. C. Chen, C. K. Sun and P.T. Chou, *Small*, 2013, **9**, 2102-2102.

12. L. Van Dao and P. Hannaford, *Nat. Photon.*, 2013, **7**, 771-772.

13. Z. Cai, Z. Xiong, J. Teng and X. Lu, *J. Mater. Chem. A*, 2014, **2**, 545-553

14. P. Herves, M. Perez-Lorenzo, L. M. Liz-Marzan, J. Dzubiella, Y. Lu and M. Ballauff, *Chem. Soc. Rev.*, 2012, **41**, 5577-5587.

15. A. Kumar, D. Saxena and M. K. Gupta, *Green Chem*, 2013, **15**, 2699-2703.

16. M. Zhu, C. Wang, D. Meng and G. Diao, *J. Mater. Chem. A*, 2013, **1**, 2118-2125.

17. D. H. Zhang, G. D. Li, J. X. Li and J. S. Chen, *Chem. Commun.*, 2008, 3414-3416.

18. R. B. Nasir Baig and R. S. Varma, *Green Chem*, 2013, **15**, 398-417.

19. M. B. Gawande, A. K. Rathi, I. D. Nogueira, R. S. Varma and P. S. Branco,

Green Chem, 2013, **15**, 1895-1899.

20. R. K. Sharma, Y. Monga, A. Puri and G. Gaba, *Green Chem*, 2013, **15**, 2800-2809.

21. V. S. Coker, J. A. Bennett, N. D. Telling, T. Henkel, J. M. Charnock, G. van der Laan, R. A. D. Pattrick, C. I. Pearce, R. S. Cutting, I. J. Shannon, J. Wood, E. Arenholz, I. C. Lyon and J. R. Lloyd, *ACS Nano*, 2010, **4**, 2577-2584.

22. C. Zhu, L. Han, P. Hu and S. Dong, *Nanoscale*, 2012, **4**, 1641-1646.

23. F. Zhang, J. Jin, X. Zhong, S. Li, J. Niu, R. Li and J. Ma, *Green Chem*, 2011, **13**, 1238-1243.

24. X. Zheng, L. Zhang, J. Li, S. Luo and J.-P. Cheng, *Chem. Commun.*, 2011, **47**, 12325-12327.

25. C. G. Frost and L. Mutton, *Green Chem*, 2010, **12**, 1687-1703.

26. D. He, S. Mu and M. Pan, *Carbon*, 2011, **49**, 82-88.

27. X. Chen, G. Wu, J. Chen, X. Chen, Z. Xie and X. Wang, *J. Am. Chem. Soc.*, 2011, **133**, 3693-3695.

28. P. Zhang, C. Shao, Z. Zhang, M. Zhang, J. Mu, Z. Guo and Y. Liu, *Nanoscale*, 2011, **3**, 3357-3363.

29. B. Dong, D. L. Miller and C. Y. Li, *J. Phys. Chem. Lett.*, 2012, **3**, 1346-1350.

30. X. Lu, X. Bian, G. Nie, C. Zhang, C. Wang and Y. Wei, *J. Mater. Chem*, 2012, **22**, 12723-12730.

31. G. Prieto, J. Zečević, H. Friedrich, K. P. de Jong and P. E. de Jongh, *Nat. Mater.*, 2013, **12**, 34-39.

32. N. Zhang and Y.-J. Xu, *Chem. Mater.*, 2013, **25**, 1979-1988.

33. S. Y. Huang, P. Ganesan and B. N. Popov, *ACS Catalysis*, 2012, **2**, 825-831.

34. S. K. Das, M. M. R. Khan, A. K. Guha and N. Naskar, *Green Chem*, 2013, **15**, 2548-2557.

35. R. B. N. Baig and R. S. Varma, *Green Chem*, 2013, **15**, 1839-1843.

36. J. Wu, N. Zhao, X. Zhang and J. Xu, *Cellulose*, 2012, **19**, 1239-1249.

37. J. Sun, J. Wang, W. Cheng, J. Zhang, X. Li, S. Zhang and Y. She, *Green Chem*, 2012, **14**, 654-660.

38. J. G. Fernandez and D. E. Ingber, *Adv. Funct. Mater*, 2013, **23**, 4454-4466.

39. S. Ladet, L. David and A. Domard, *Nature*, 2008, **452**, 76-79.

40. D. H. Bartlett and F. Azam, *Science*, 2005, **310**, 1775-1777.

41. C. K. S. Pillai, W. Paul and C. P. Sharma, *Prog. Polym. Sci.*, 2009, **34**, 641-678.

42. J. Jin, P. Hassanzadeh, G. Perotto, W. Sun, M. A. Brenckle, D. Kaplan, F. G. Omenetto and M. Rolandi, *Adv. Mater.*, 2013, **25**, 4482-4487.

43. M. Poirier and G. Charlet, *Carbohyd Polym*, 2002, **50**, 363-370.

44. H. Tamura, H. Nagahama and S. Tokura, *Cellulose*, 2006, **13**, 357-364.

45. S. S. Silva, A. R. C. Duarte, J. F. Mano and R. L. Reis, *Green Chem*, 2013, **15**, 3252-3258.

46. C. Chang, S. Chen and L. Zhang, *J. Mater. Chem.*, 2011, **21**, 3865-3871.

47. B. Ding, J. Cai, J. Huang, L. Zhang, Y. Chen, X. Shi, Y. Du and S. Kuga, *J. Mater. Chem.*, 2012, **22**, 5801-5809.

48. B. Duan, C. Chang, B. Ding, J. Cai, M. Xu, S. Feng, J. Ren, X. Shi, Y. Du and L. Zhang, *J. Mater. Chem. A*, 2013, **1**, 1867-1874.

49. H. Tang, C. Chang and L. Zhang, *Chem. Eng. J.*, 2011, **173**, 689-697.

50. M. R. Kasaai, *Carbohyd. Polym.*, 2008, **71**, 497-508.

51. X. Luo, S. Liu, J. Zhou and L. Zhang, *J. Mater. Chem.*, 2009, **19**, 3538-3545.

52. D. Horák, M. Babič, H. Macková and M. J. Beneš, *J. Sep. Sci.*, 2007, **30**, 1751-1772.

53. X. Luo and L. Zhang, *J. Chromatogr. A*, 2010, **1217**, 5922-5929.

54. M. Kruk and M. Jaroniec, *Chem. Mater.*, 2001, **13**, 3169-3183.

55. J. Liu, Z. Zhao, H. Feng and F. Cui, *J. Mater. Chem.*, 2012, **22**, 13891-13894.

56. J. Mu, B. Chen, Z. Guo, M. Zhang, Z. Zhang, P. Zhang, C. Shao and Y. Liu, *Nanoscale*, 2011, **3**, 5034-5040.

57. D. Zhang, Z. Liu, S. Han, C. Li, B. Lei, M. P. Stewart, J. M. Tour and C. Zhou, *Nano Letters*, 2004, **4**, 2151-2155.

58. Z. Zhang, J. Zhang, B. Zhang and J. Tang, *Nanoscale*, 2013, **5**, 118-123.

59. D. Oh, S. Shin, C. Lim and D. Hwang, *Materials*, 2013, **6**, 3826-3839.

60. J. R. Oliveira, M. C. L. Martins, L. Mafra and P. Gomes, *Carbohyd. Polym*, 2012, **87**, 240-249.

61. Z. Geng, Y. Lin, X. Yu, Q. Shen, L. Ma, Z. Li, N. Pan and X. Wang, *J. Mater. Chem*, 2012, **22**, 3527-3535.

62. Y. Sun, L. Xu, Z. Yin and X. Song, *J. Mater. Chem. A.*, 2013, **1**, 12361-12370.

63. Y. Lin, Y. Qiao, Y. Wang, Y. Yan and J. Huang, *J. Mater. Chem.*, 2012, **22**,

18314-18320.

64. L. Ai, H. Yue and J. Jiang, *J. Mater. Chem.*, 2012, **22**, 23447-23453.

65. H. Tang, L. Zhang, L. Hu and L. Zhang, *J. Plant. Growth. Regul.*, 2013, 1-7.

Figure captions

Table 1 Surfaces properties of RChS and MRChS.

Scheme 1 Schematic depiction for in situ synthesis of Ag-Fe_3O_4 nanocomposites on the chitin microspheres: "living" chitin microspheres with surface-bound acetyl amine groups in nano-sized pores (a); $Fe(OH)_2$ (b) and Ag-Fe_3O_4 (c) nanoparticles anchored with the acetyl amine groups of chitin microspheres.

Fig. 1 Optical photomicrgraphs of the RChS (a) and MRChS (c), the scale bar is 300 μm and the size distribution of RChS (b) and M30 (d) observed with the laser particle size analyzer.

Fig. 2 SEM images of the RChS (a), M15 (b), M30 (c) and M45 (d). The scale bar is 50μm.

Fig. 3 Nitrogen adsorption and desorption isotherms (a) and Barrett-Joyner-Halendar (BJH) pore size distribution (b) of RChS, M15, M30, and M45.

Fig. 4 TEM images of the magnetic microspheres of M15 (a), M30 (b) and M45 (c). HRTEM of an individual particle and the lattice fringes marked (d). Typical EDS spectrum of the particle from HRTEM (e).

Fig. 5 XPS fully scanned spectra of RChS and M30 (a); XPS spectra of Ag 3d (b) and Fe 2p (c) for M30; XPS spectrum of N1s (d), C1s (e) and O1s (f) for RChS and M30, respectively.

Fig. 6 Magnetic hysteresis loops and enlarged view (inset) of the central portion of M15, M30 and M45 (a), and photographs of the MRChS dispersion in water (b), and

the attraction behaviors induced by the magnet immersed in the water for 5 sec (c), 13 sec (d).

Fig. 7 Catalytic performances of the MRChS on 4-NP: UV–vis absorption spectra during the catalytic reduction of 4-NP over M30 (50 mg/L) (a); the inserts are the reaction scheme associated color change from bright yellow of 4-NP to colorless 4-AP; Plots of the absorbance at 400 nm for ln(C/Co) (b) and C/Co (c) versus the reduction reaction time for 4-NP, M15, M30 and M45 at the concentration of 50 mg/L, the control experiment (50mg/L chitin microspheres); Catalytic activity of the sample M30 (50 mg/L) for 4-NP with 10 times of cycling uses as a function of time (d).

Fig. 8 Optical photograph of the preparative chromatography column packed with MRChS for the catalytic reaction from 4-nitrophenol to 4-aminophenol.

669 **Table 1** Surfaces properties of RChS and MRChS.

670

Sample	Structural parameters		
	Surface area (m^2/g)	Pore volume ($cm^3\ g^{-1}$)	Pore size (nm)
RChS	34.6	0.252	22.3
M15	33.1	0.124	14.1
M30	32.5	0.157	15.3
M45	18.8	0.084	26.2

671
672
673
674
675
676
677
678
679
680
681
682
683
684
685
686
687
688
689
690
691
692

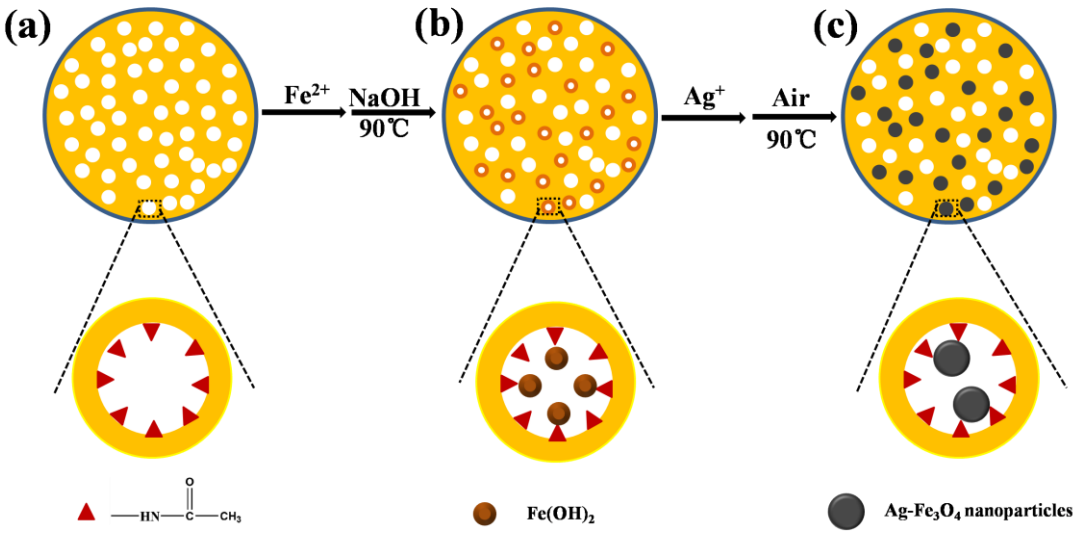

693

694 **Scheme 1** Schematic depiction for in situ synthesis of Ag-Fe_3O_4 nanocomposites on

695 the chitin microspheres: "living" chitin microspheres with surface-bound acetyl amine

696 groups in nano-sized pores (a); $Fe(OH)_2$ (b) and Ag-Fe_3O_4 (c) nanoparticles anchored

697 with the acetyl amine groups of chitin microspheres.

698

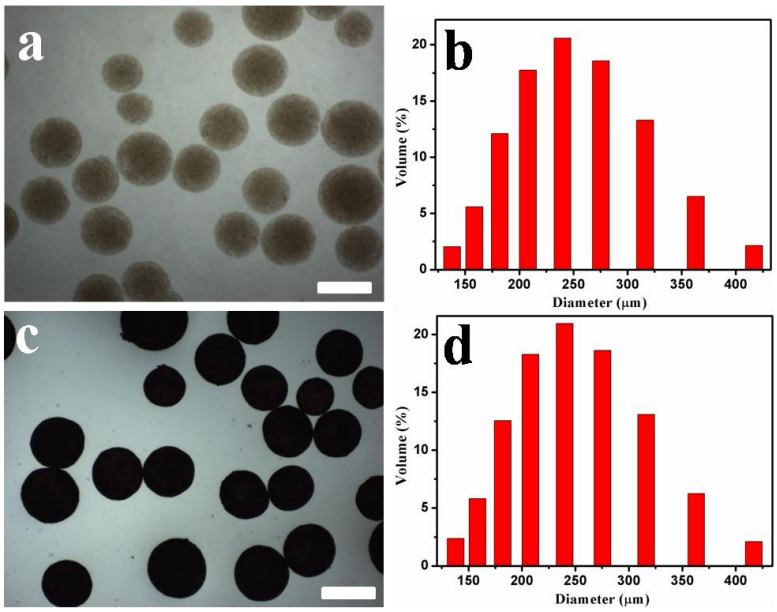

699
700

701 **Fig. 1** Optical photomicrgraphs of the RChS (a) and MRChS (c), the scale bar is 300

702 μm and the size distribution of RChS (b) and M30 (d) observed with the laser particle

703 size analyzer.

704

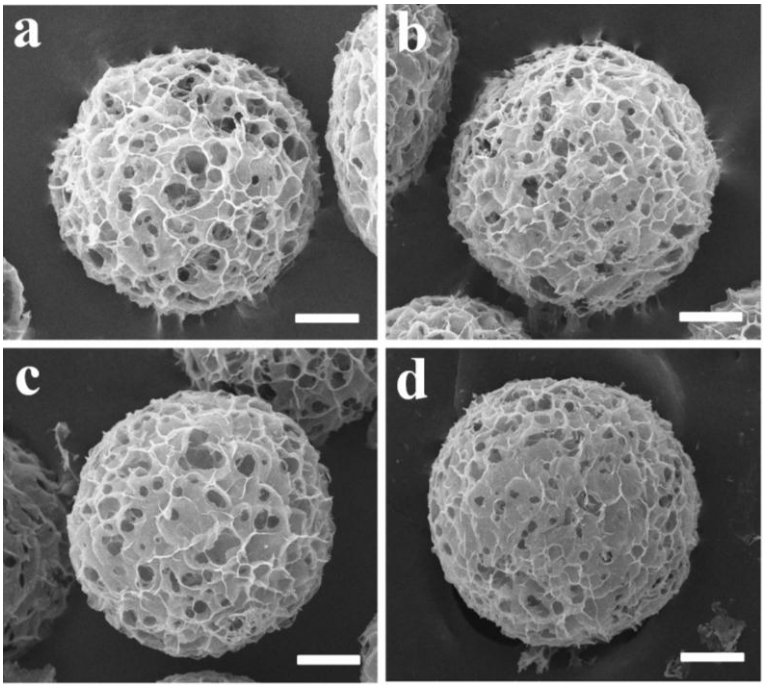

Fig. 2 SEM images of the RChS (a), M15 (b), M30 (c) and M45 (d). The scale bar is 50μm.

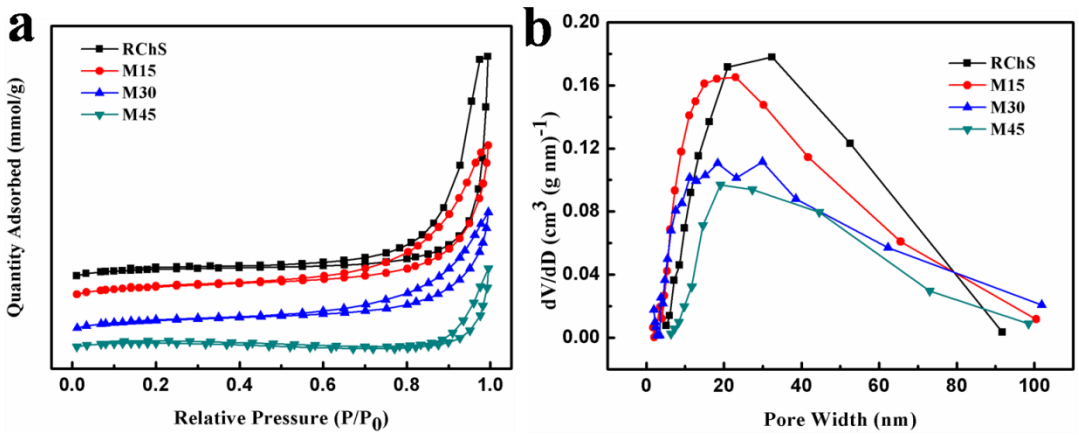

Fig. 3 Nitrogen adsorption and desorption isotherms (a) and Barrett-Joyner-Halendar (BJH) pore size distribution (b) of RChS, M15, M30, and M45.

715

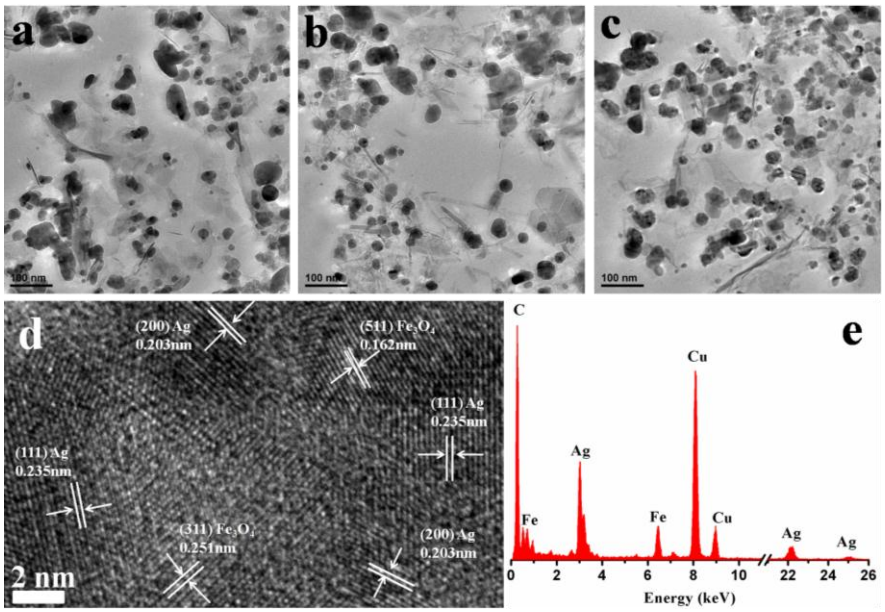

716

717

718 **Fig. 4** TEM images of the magnetic microspheres of M15 (a), M30 (b) and M45 (c).

719 HRTEM of an individual particle and the lattice fringes marked (d). Typical EDS

720 spectrum of the particle from HRTEM (e).

721

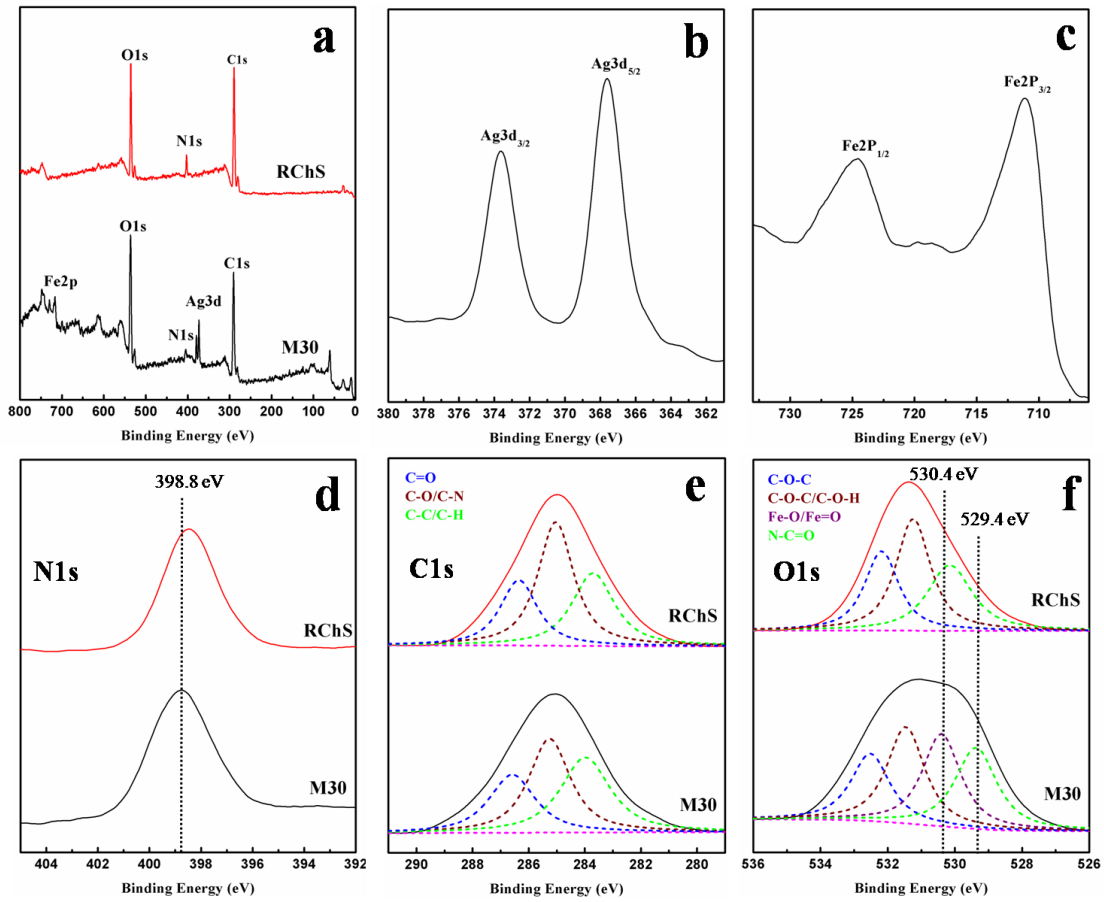

Fig. 5 XPS fully scanned spectra of RChS and M30 (a); XPS spectra of Ag 3d (b) and Fe 2p (c) for M30; XPS spectrum of N1s (d), C1s (e) and O1s (f) for RChS and M30, respectively.

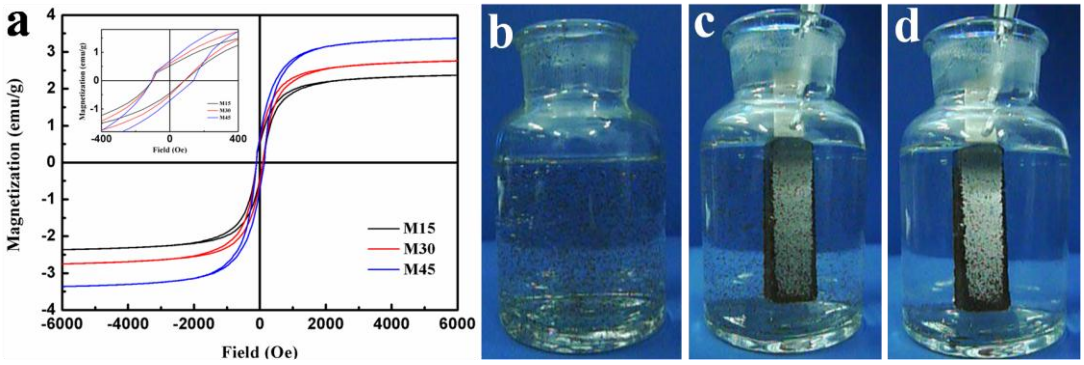

Fig. 6 Magnetic hysteresis loops and enlarged view (inset) of the central portion of M15, M30 and M45 (a), and photographs of the MRChS dispersion in water (b), and the attraction behaviors induced by the magnet immersed in the water for 5 sec (c), 13 sec (d).

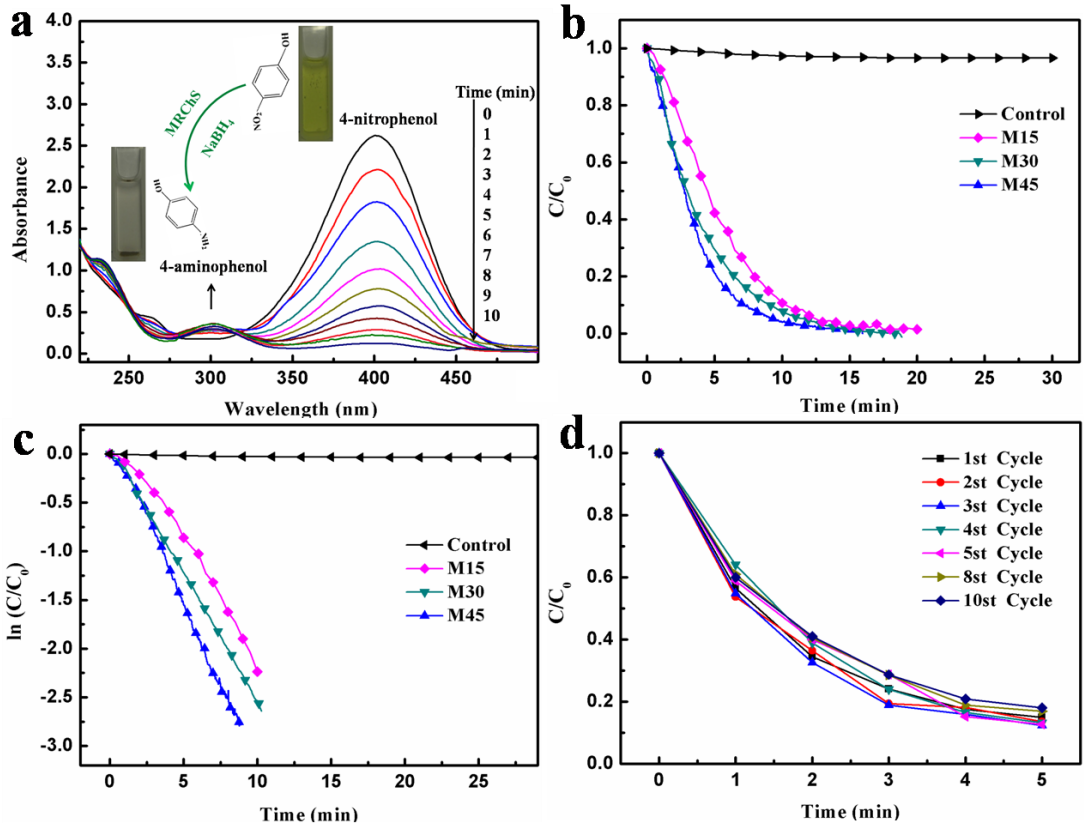

740

741 **Fig. 7** Catalytic performances of the MRChS on 4-NP: UV–vis absorption spectra
742 during the catalytic reduction of 4-NP over M30 (50 mg/L) (a); the inserts are the
743 reaction scheme associated color change from bright yellow of 4-NP to colorless
744 4-AP; Plots of the absorbance at 400 nm for ln(C/Co) (b) and C/Co (c) versus the
745 reduction reaction time for 4-NP, M15, M30 and M45 at the concentration of 50 mg/L,
746 the control experiment (50mg/L chitin microspheres); Catalytic activity of the sample
747 M30 (50 mg/L) for 4-NP with 10 times of cycling uses as a function of time (d).

748

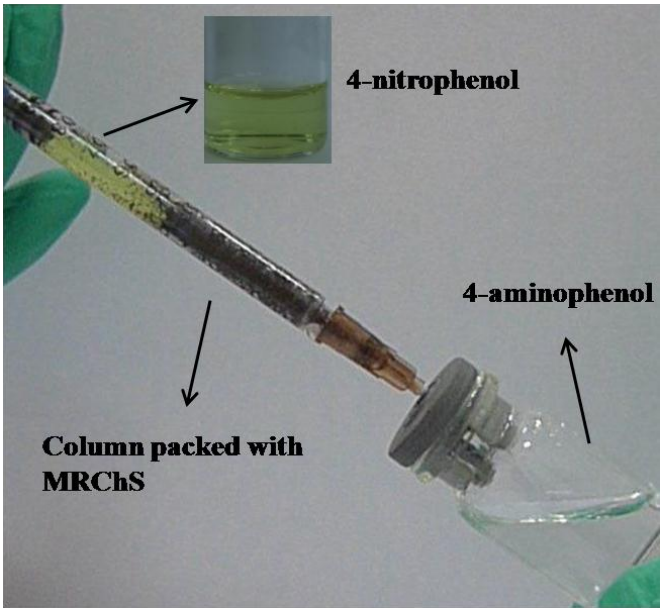

Fig. 8 Optical photograph of the preparative chromatography column packed with MRChS for the catalytic reaction from 4-nitrophenol to 4-aminophenol.